

Data selection.

We use the earthquake catalogue recorded during the aftershock sequence of the 2009 L'Aquila earthquake at a very dense seismic network of 60 stations operating for 9 months after the M_w 6.1 mainshock, composed by about 64k precisely located aftershocks (inset to the left in Fig. 1; Valbroso et al, 2013). Data were analysed by combining an accurate automatic picking procedure for P- and S-waves (Aldersons et al, 2009), together with cross-correlation and double-difference location methods (Waldhauser and Schaff, 2008) reaching a completeness magnitude (i.e. the minimum magnitude above which all the events occurring in a study area can be reliably detected and located; Weimer and Wyss, 2000) equal to 0.7, which corresponds to a source dimension of ~ 50 m based on a circular crack model using a 3 MPa stress drop. Earthquake relative location errors are in the range of a few meters to tens of meters (i.e., the error ellipsoids obtained at the 95% confidence level for 200 bootstrap samples show median values of the distribution along the major/minor horizontal and vertical direction of 24, 15 and 27 m; see Valbroso et al., 2013 for details). These errors are comparable to the spatial dimension of the earthquakes themselves, allowing us to confidently image the internal structure of the fault zone down to the tens of meter scale.

We select from the entire earthquake catalogue those aftershocks nucleating on the causative fault of the M_w 6.1 L'Aquila mainshock (black dots in Figure 1). With this aim, we choose all earthquakes occurring within 6 km (+/- 3 km) from the AF plane as modelled by inverting strong motion, GPS and DInSAR data (Cirella et al., 2012). This plane is 20-km-long along the N133°E striking direction and dips 54° to SW, intersecting the mainshock hypocentre (the projection at the surface of this plane is shown as a red box in the map in Figure 1). The resulting catalogue is made of ~ 19 k aftershocks (black dots in Figure 1).

Fault zone thickness estimation. catalogue computed by Chiaraluce et al., (2011) and shown for details of fault zone representative events in Fig. 2 of the manuscript. To investigate the details of fault zone representative events beneath the AF, we divide the 20-km-long volume in forty (40) 500-m-wide vertical boxes (NW-trending black traces in Fig. 1 of the manuscript). All the 40 vertical sections reporting the earthquake distribution at depth are shown in Fig. DR1. For each cross-section, we compute

the number of aftershocks occurring every 50 m within 6 km (± 3) of distance perpendicularly to the fault plane modelled by Cirella et al. (2012; red dotted lines in the cross-sections) and we build histograms describing the detailed earthquake occurrence around the fault plane (histograms in Fig. DR1).

In order to exclude the portion of the fault characterized by multiple fault strands at shallow depth, which might complicate the interpretation of our results, we include only aftershocks occurring at depths larger than 4 km. Negative and positive distances in the histogram indicate the footwall and the hanging-wall block, respectively. Almost all the histograms show a Gaussian distribution of the earthquakes. Thus, we define the damage zone thickness (DZT) as 2 times the standard deviation of the distribution (i.e., 95% of the aftershocks).

Damage density decay estimation.

We measure the fault-normal earthquake density decay (i.e. the number of earthquakes occurring every 50 m) as a function of distance from the fault plane. We find that the decay is well fit by a power-law function in agreement with numerous geological (e.g. Savage and Brodsky, 2011) and seismological (e.g. Powers and Jordan, 2010; Hauksson, 2010) data. Then, we compute the decay exponent (n) by plotting our data in a log-log scale and fitting the data using a least squares method for both the footwall and hanging-wall block (Fig. DR2A and DR2B, respectively). The slope of the linear regression (black dotted line in Fig. DR2) represents the earthquake decay exponent of the power-law function.

Fault zone thickness and mainshock rupture evolution.

We compared the fault zone thickness with the mainshock rupture evolution both in terms of coseismic slip distribution (see Fig. 4 of the main manuscript) and rupture velocity. In Fig DR3, we show the local rupture velocity distribution computed by Cirella et al., (2012) on the fault plane of the 2009 L'Aquila main shock overlapped by the slip contour (white line, in metres) and the seismicity occurring within 6 km (± 3) of distance perpendicularly to the fault plane. Fig. DR3 shows how at the SE end of the fault, the rupture front stopped where the geometry of the fault becomes complex, indicating that off-fault damage strongly influences the arrest of the earthquake rupture propagation.

REFERENCES CITED.

- Aldersons, F., Di Stefano, R., Chiaraluca, L., Piccinini, D. and Valeroso, L., 2009, Automatic detection, and P and S wave picking algorithm: An application to the 2009 L'Aquila (central Italy) earthquake sequence: *Eos Trans. AGU*, 90(52).
- Chiaraluca, L., Valeroso, L., Piccinini, D., Di Stefano, R., and De Gori, P., 2011, The anatomy of the 2009 L'Aquila normal fault system (central Italy) imaged by high resolution foreshock and aftershock locations: *Journal of Geophysical Research*, v. 116 (B12311).
- Cirella, A., Piatanesi, A., Tinti, E., Chini, M. and Cocco, M., 2012, Complexity of the rupture process during the 2009 L'Aquila, Italy, earthquake: *Geophysical Journal International*, v. 190, p. 607–621.
- Hauksson, E., 2010, Spatial separation of large earthquakes, aftershocks, and background seismicity: analysis of interseismic and coseismic seismicity patterns in southern California: *Pure and Applied Geophysics*, v. 167, p. 979–997.
- Powers, P. M. and Jordan T. H., 2010, Distribution of seismicity across strike-slip faults in California: *Journal of Geophysical Research*, v. 115 (B05305).
- Savage, H.M. and Brodsky, E.E., 2011, Collateral damage: Evolution with displacement of fracture distribution and secondary fault strands in fault damage zones: *Journal of Geophysical Research*, v. 116 (B03405).
- Valeroso, L., Chiaraluca, L., Piccinini, D., Di Stefano, R., Schaff, D. and Waldhauser, F., 2013, Radiography of a normal fault system by 64,000 high-precision earthquake locations: the 2009 L'Aquila (central Italy) case study: *Journal of Geophysical Research*, v. 118.
- Waldhauser, F. and Schaff, D. P., 2008, Large-scale relocation of two decades of Northern California seismicity using cross-correlation and double-difference methods: *Journal of Geophysical Research*, v. 113 (B08311).
- Wiemer, S., and Wyss, M., 2000, Minimum magnitude of complete reporting in earthquake catalogs: Examples from Alaska, the Western United States, and Japan: *Seismological Society of America Bulletin*, v. 90, p. 859–869.

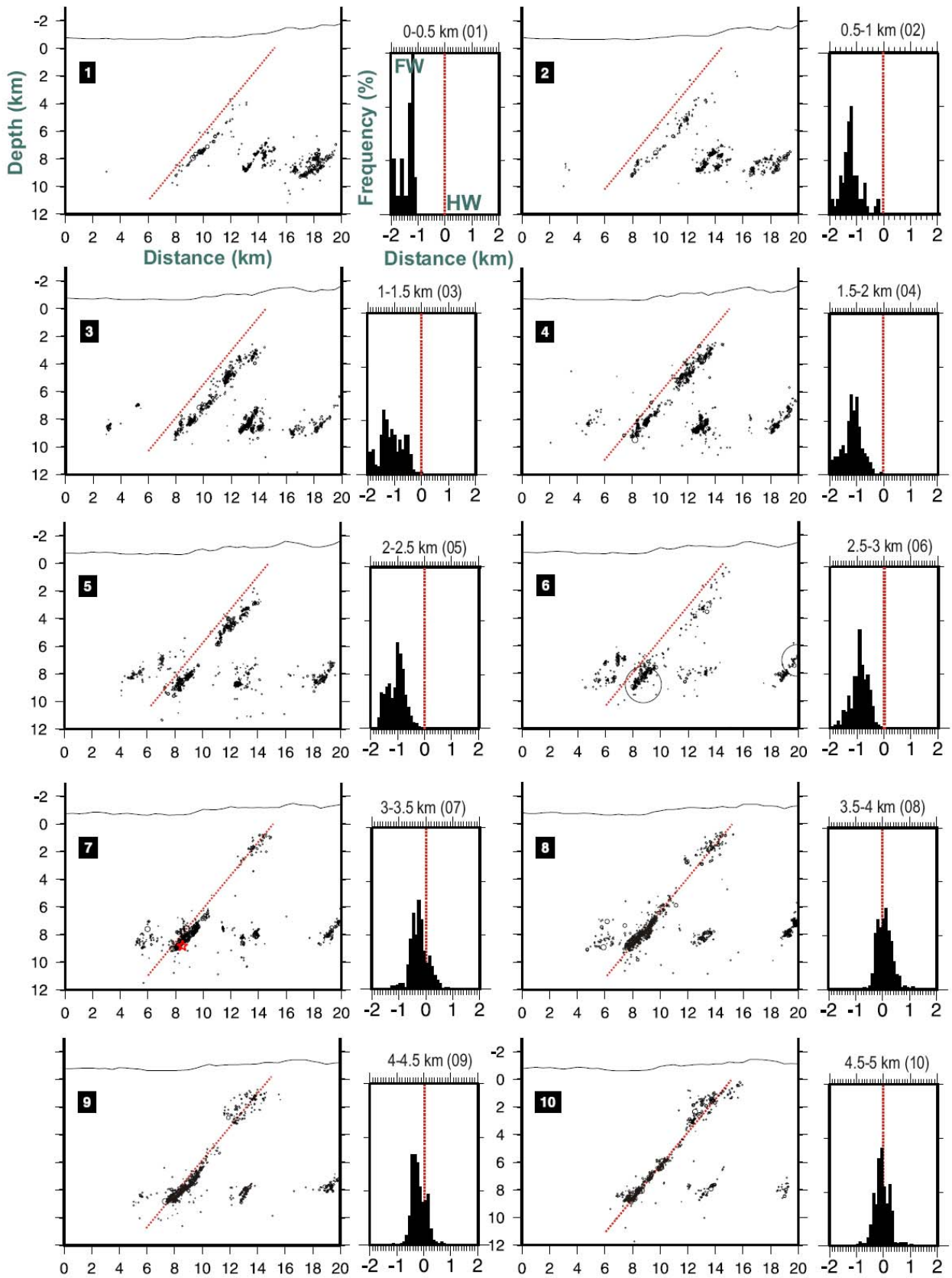


Figure DR1: NE-trending vertical sections (1-40) showing: the aftershocks distribution (black dots scaled to represent the approximate source dimension assuming a 3 MPa circular constant stress drop source); the projection at depth of the coseismic rupture plane computed by Cirella et al. (2012; red dotted line); the hypocentral location of the largest magnitude events (red stars). For each cross-section we also report a histogram showing the number of earthquakes occurring every 50 m within 6 km (\pm 3 km) of distance perpendicularly to the modelled fault plane (Cirella et al., 2012).

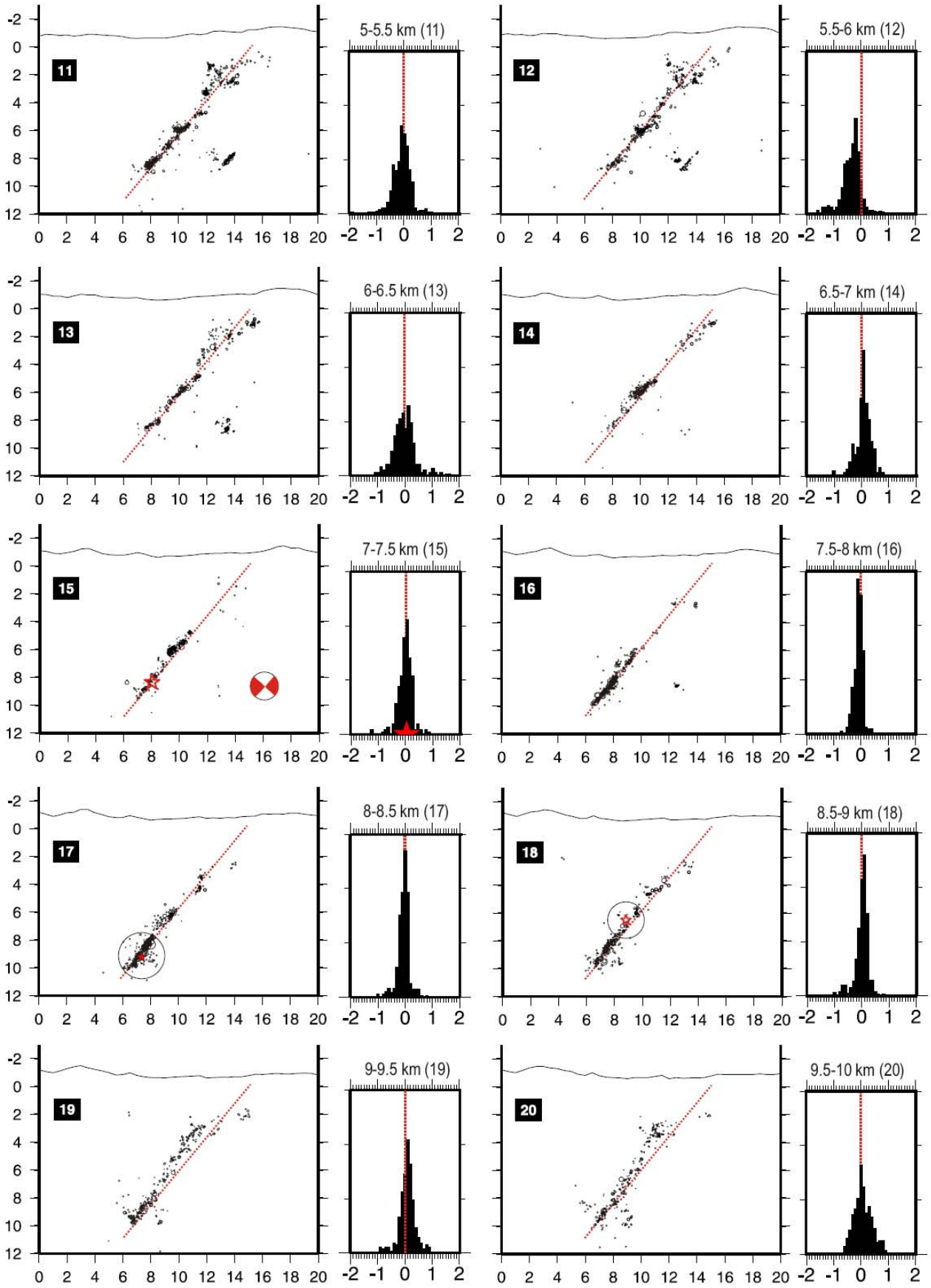


Figure DR1 (continues)

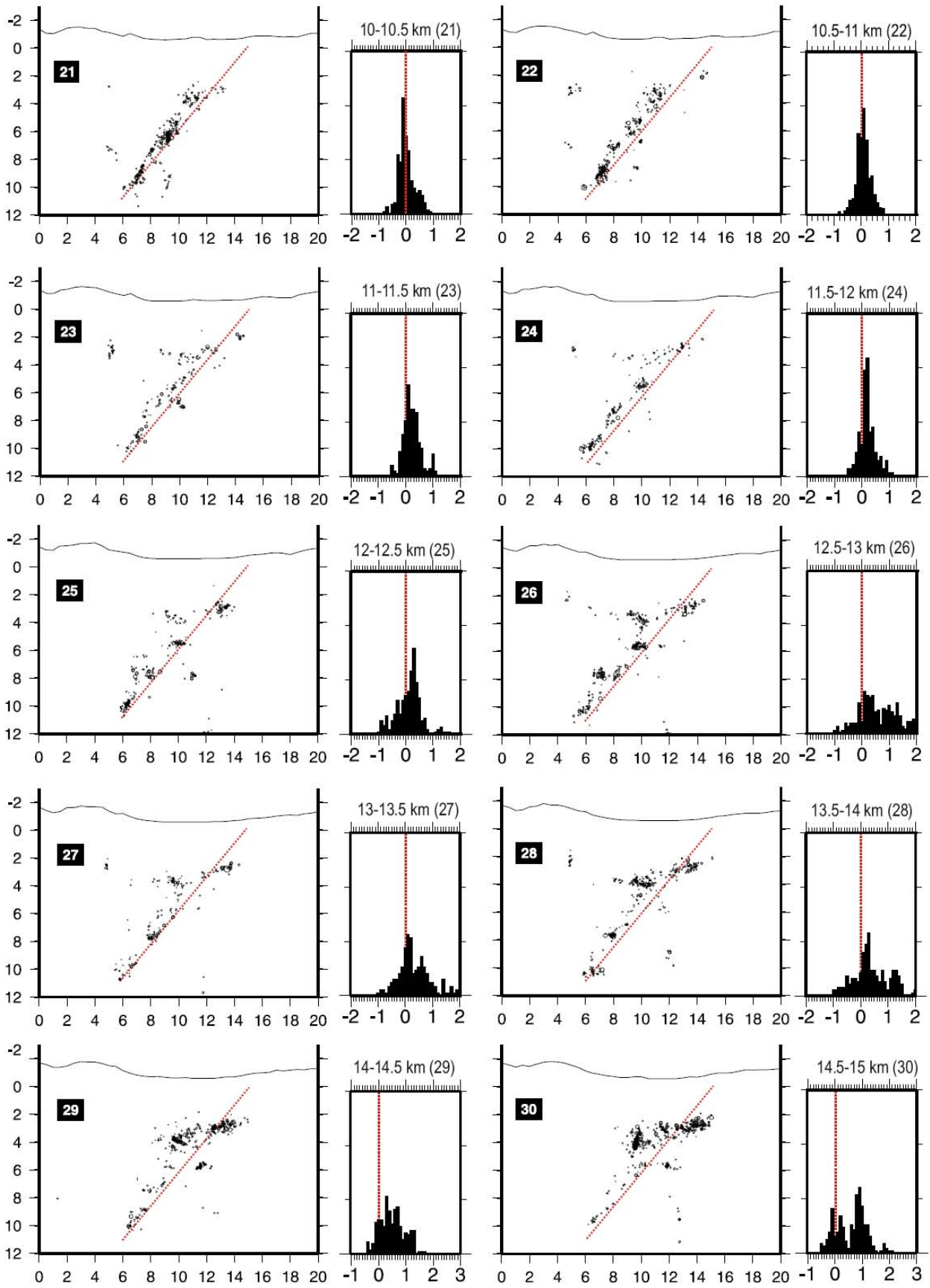


Figure DR1 (continues)

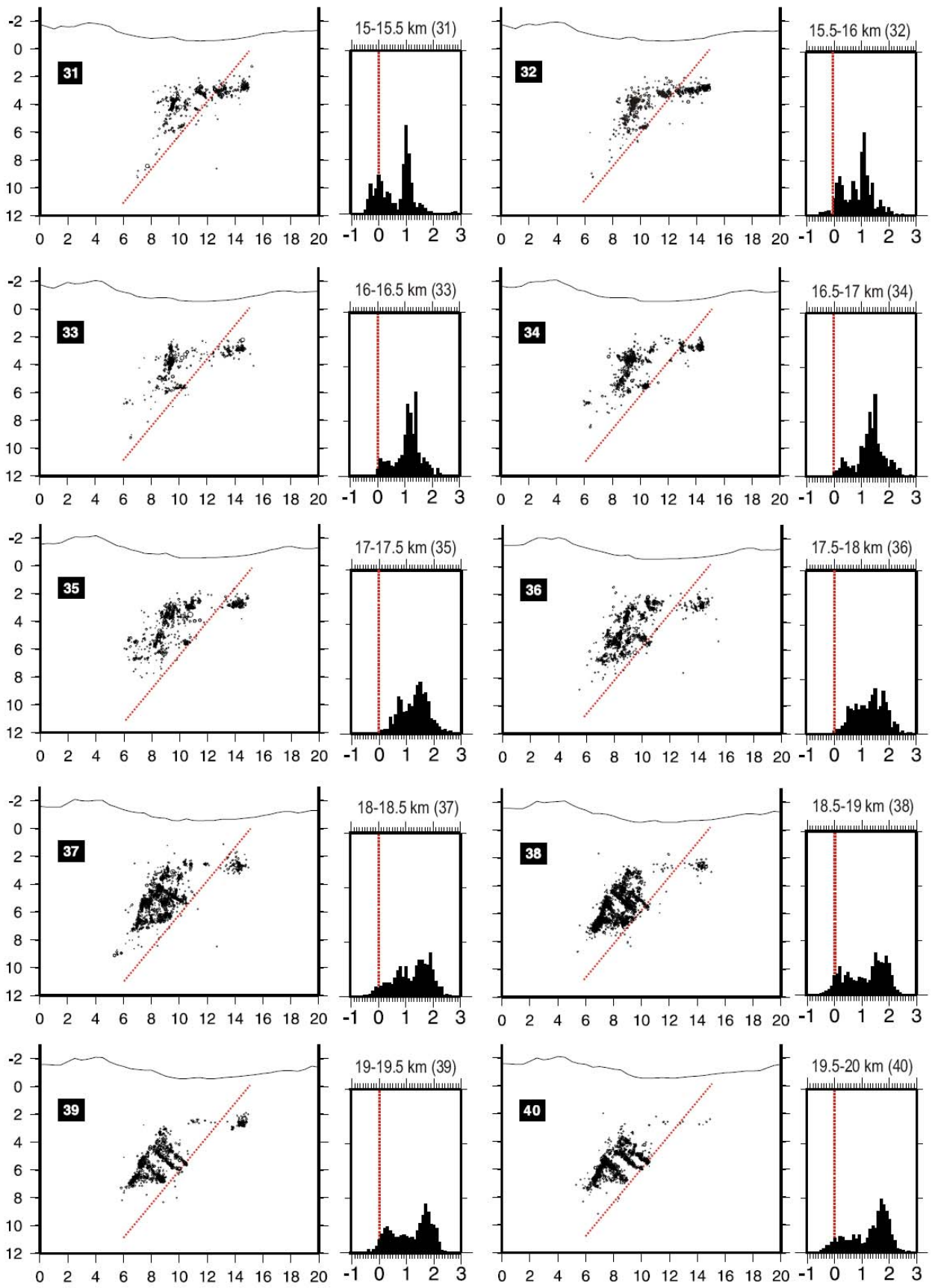


Figure DR1.

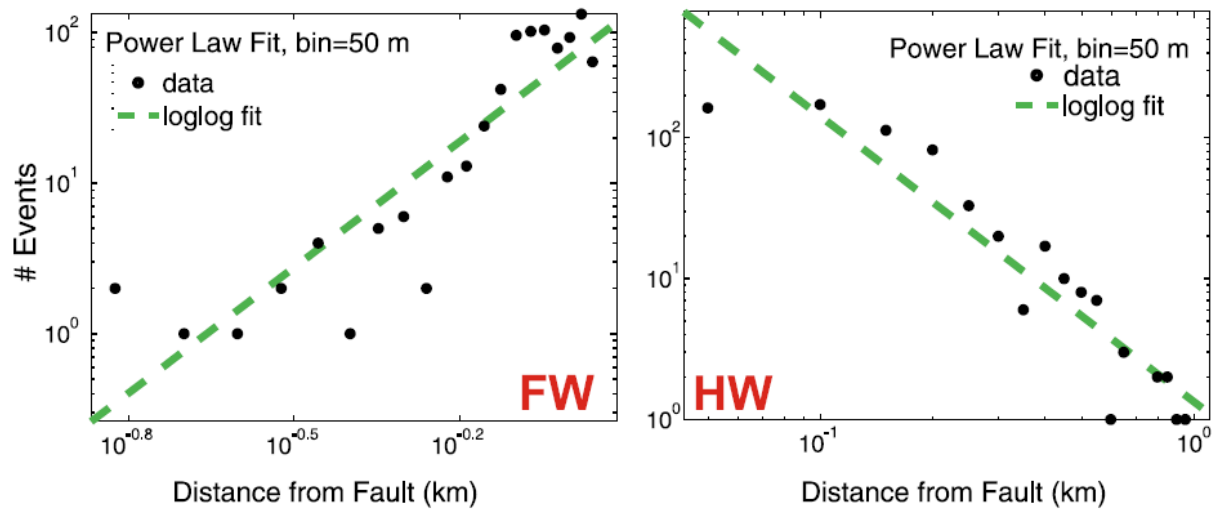


Figure DR2: Logarithmic plots of the fault normal earthquake density distribution (black dots) for (A) footwall and (B) hanging-wall block, with the computed linear fit of the distribution (grey dotted line). The slope of the line is the decay exponent (n) of the power-law function, while R represents the quality of the fit.

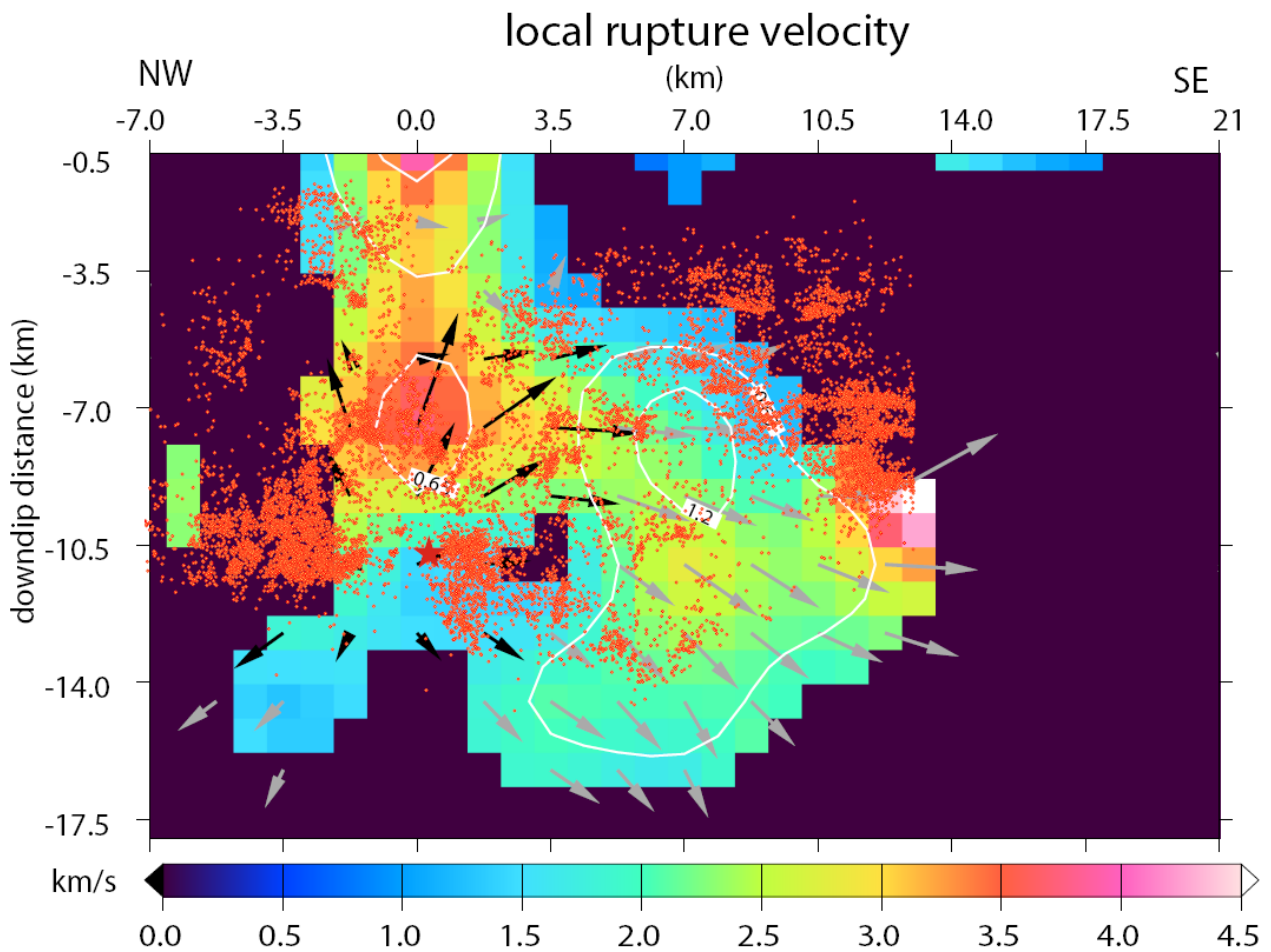


Figure DR3: Local rupture velocity distribution on the fault plane for the 2099 L'Aquila main shock overlapped by the slip contour (white line, in metres), by the rupture velocity vectors (black and grey arrows show the rupture velocity vector for rupture times between 0 and 2.0 s and over 2.0 s, respectively) and by the aftershocks occurring within 6 km (\pm 3 km) from the fault plane. Modified after Cirella et al., (2012).